Journal of
Applied Remote Sensing

RemoteSensing.SPIEDigitalLibrary.org

Predicting leaf chlorophyll content and its nonuniform vertical distribution of summer maize by using a radiation transfer model

Xiaobin Xu
Zhenhai Li
Xiaodong Yang
Guijun Yang
Cong Teng
Hongchun Zhu
Shuaibing Liu

SPIE.

Xiaobin Xu, Zhenhai Li, Xiaodong Yang, Guijun Yang, Cong Teng, Hongchun Zhu, Shuaibing Liu, "Predicting leaf chlorophyll content and its nonuniform vertical distribution of summer maize by using a radiation transfer model," *J. Appl. Remote Sens.* **13**(3), 034505 (2019), doi: 10.1117/1.JRS.13.034505.

Predicting leaf chlorophyll content and its nonuniform vertical distribution of summer maize by using a radiation transfer model

Xiaobin Xu,[a,b] Zhenhai Li,[b] Xiaodong Yang,[b] Guijun Yang,[b] Cong Teng,[a,b] Hongchun Zhu,[a,*] and Shuaibing Liu[b]

[a]Shandong University of Science and Technology, College of Geomatics, Qingdao, China
[b]Ministry of Agriculture P. R. China, Key Laboratory of Quantitative Remote Sensing in Agriculture, Beijing Research Center for Information Technology in Agriculture, Beijing, China

Abstract. Remote sensing technology is an effective method of monitoring chlorophyll content, an important parameter for vegetation health. The chlorophyll information based on spectral information needs to consider the vertical characteristics of plants. Hyperspectral features [spectral reflectance (SR), spectral indices, and wavelet coefficients (WC)] were first selected to construct the cost function in the PROSPECT model-optimized inversion to improve the accuracy and efficiency of leaf chlorophyll content (LCC) inversion. Second, the sensitivity of LCC to leaf SR, vegetation index (*VI*), and WC were analyzed. Finally, LCC was inverted by the PROSPECT model using the iterative inversion algorithm, and the chlorophyll content of the vertical profile in maize was monitored. The following results were obtained. (1) According to the extended Fourier amplitude sensitivity test (EFAST) used to construct the cost-function inversion of LCC, the normalized difference vegetation index canste ($NDVI_{canste}$) and WC based on EFAST method which was used to construct the cost-function inversion of LCC, yielded higher accuracy than other spectral features. These two methods, combined with sensitivity analysis can provide accurate inversion results by weakening the influence of other parameters on spectral changes and eliminating the interference information between bands. (2) The cost function based on $NDVI_{canste}$ in the LCC optimization exhibited overestimation, whereas WC can solve the problem efficiently. The continuous wavelet transform can extract weak information among the spectra, whereas the other two methods of SR and VI cannot easily obtain this information. (3) The vertical distribution of LCC in different maize varieties and treatments is in accordance with the parabola law, but the chlorophyll content of the different leaf positions on the vertical profile is somewhat different. The results reflect the vertical distribution of chlorophyll content through the radiation transfer of leaves, thus providing a theoretical basis for their further combination. [DOI: 10.1117/1.JRS.13.034505]

Keywords: PROSPECT-D; chlorophyll; sensitivity; continuous wavelet transform; vertical distribution.

Paper 190041 received Jan. 19, 2019; accepted for publication Jul. 3, 2019; published online Jul. 22, 2019.

1 Introduction

Chlorophyll is a good indicator of photosynthesis ability, physiological stress, carbon sequestration capacity, and efficient nitrogen use of vegetation.[1] Hyperspectral remote sensing technology is a simple, rapid, effective, and nondestructive data acquisition and processing method that directly and quantitatively analyzes the weak spectral differences of vegetation and has shown advantages in vegetation remote sensing research and application.[2,3] Therefore, the rapid and timely monitoring of leaf chlorophyll content (LCC) at different growth stages by using hyperspectral remote sensing has an essential role in crop growth and yield estimation.[4] Plant growth and development, nitrogen absorption and reactivation, and distribution of chlorophyll

*Address all correspondence to Hongchun Zhu, E-mail: sdny_xa@163.com

1931-3195/2019/$28.00 © 2019 SPIE

content in plant leaves in the vertical profile are not uniform due to the different processes of light in the environment.[5] This phenomenon is seldom considered in remote sensing monitoring, leading to limitations in monitoring accuracy and decline of practical applications.

The methods of obtaining crop LCC through remote sensing data are mainly divided into empirical/semiempirical statistical and physical model inversion methods.[6] Empirical statistical methods are mainly based on the statistical regression model and are used to establish a regression equation between spectral reflectance (SR) and LCC. Semiempirical statistical methods focus on the development of vegetation index (VI), which is highly correlated with LCC and is not sensitive to other interference factors. Sims and Gamon[7] used spectral indices constructed by using the characteristic bands of 550 and 700 nm to invert the LCC and finally obtained relatively high estimation accuracy. Pisek and Chen[8] pointed out that various forms of spectral indices based on ground or aerospace sensors could be used to estimate crop blade LCC. Wu et al.[9] considered the spectral information of red edge position (705 and 750 nm) in the construction of spectral index, and finally presented a reliable estimate for wheat LCC. However, empirical and semiempirical statistical methods lack robustness and portability.

Jacquemoud and Baret[10] proposed the LCC-based radiation transmission model PROSPECT, which can accurately simulate the hemispherical reflectivity and transmittance of different plant leaves (monocotyledonous, dicotyledonous, and old leaves) from 400 to 2500 nm. This study was based on the most advanced PROSPECT-D[11] model. However, the physical inversion model uses the sensitive SR and VI as the optimization comparison features for the cost function in the inversion algorithm in the main, thereby resulting in data redundancy and low inversion efficiency. Wei et al.[12] constructed the cost function of the inversion algorithm of PROSAIL model through MSR, NDVI, and ARVI to estimate leaf area index. Camino et al.[13] combined solar-induced chlorophyll fluorescence to construct the cost function of PROSAIL. The reflectivity changes caused by different biochemical parameters concurrently appear as "overlapping" and would affect the contribution of LCC to reflectance changes, thereby reducing the accuracy of the inversion.[14]

The PROSPECT-D model is a nonlinear model with many parameters that need to be inverted; some of which are sensitive, and others are insensitive.[15] Therefore, strategic selection and whether or not all parameters are inverted together or some insensitive parameters are fixed should be considered in inversion. Parameter sensitivity analysis is the basis of strategic formulation in inversion. Model sensitivity analysis identifies and screens the main parameters, thus profoundly influencing the simulation results.[16] Sensitivity analysis could be divided into local and global sensitivity analyses.[17] Among them, the extended Fourier amplitude sensitivity test (EFAST) has substantial theoretical advantages and application potential for the parameters of global sensitivity analysis and in many geomodel studies.[18,19] In fields of vegetation remote sensing models, Zhiwei et al.[20] and Bowyer and Danson[21] used EFAST to analyze the global sensitivity of ACRM and PROSAIL model parameters, respectively. Maire et al.[22] used the EFAST method to examine the sensitivity of PROSAIL model parameters.

Continuous wavelet transform (CWT) has the advantages of time-frequency locality, multiresolution analysis, and rich wavelet basis functions and has received increasing attention in the fields of signal and image analysis, denoising, compression, and decomposition.[23] This method could effectively separate high-frequency and low-frequency signals and extract the weak information from the spectral signal. Cheng et al.[24] used CWT on the spectra of 265 leaf samples from 47 plants and successfully inverted the water content with inversion accuracy reaching 75%. Liao et al.[25] compared the spectral indices and CWT methods to estimate the LCC of maize at different nitrogen levels. The results showed that the accuracy of the estimated wavelet coefficient (WC) was higher than that of the spectral index model. Some scholars used CWT to invert the LCC content of crops, but the findings were limited to empirical relationships. The inversion of LCC content in summer maize leaves by using combined CWT and physical models is rarely studied.

The development of remote sensing technology, combined with the physical, empirical, and semiempirical methods, enables the easy estimation of LCC of crops at the field scale. However, most LCC estimates are limited to vertical heterogeneity. Lower plant leaves are greatly affected by malnutrition and senescence compared with upper leaves.[26] Wang et al.[27] showed that the nitrogen content in crops decreases from bottom to top. Guo et al.[28] found that the uneven

distribution of nutrients is important to crop growth and development. Luo et al.[29] established an estimation model of nitrogen content for the upper reed layer by using plant pigmentation ratio and normalized difference VI. The values of R^2 and RMSE were 0.88 and 0.37%, respectively. Chlorophyll distribution is essential to nitrogen change, and this information is particularly important in guiding and regulating the precision of fertilization in the field.

The objectives of this study were as follows: (1) assess the spectral characteristics (SR, VI, and WC) of sensitivity of individual biochemical parameters and consider the results in the inversion algorithm, (2) invert the LCC of summer maize based on the PROSPECT-D model, and (3) study the nonuniform vertical LCC distribution by inverting the chlorophyll information in maize.

2 Materials and Methods

2.1 *Field Experiment and Data Acquisition*

A field experiment during the 2017 growing season was conducted in the experimental field of the Xiaotangshan National Precision Agriculture Research and Demonstration Base (40°00′-40° 21′N, 116°34′-117°00′E), Changping District, Beijing (Fig. 1). The base has a temperate monsoon semihumid climate zone with an annual average temperature of 11.8°C and annual average precipitation of 550.3 mm (mainly concentrated in summer). The main types of soil in the study area are moist soil and heavy loam soil, which mainly contain nitrogen, phosphorus, potassium, and organic matter. Among these elements, nitrate nitrogen content is 3.16 to 14.82 mg/kg, total nitrogen content is 1.0 to 1.2 g/kg, available phosphorus content is 3.14 to 21.18 mg/kg,

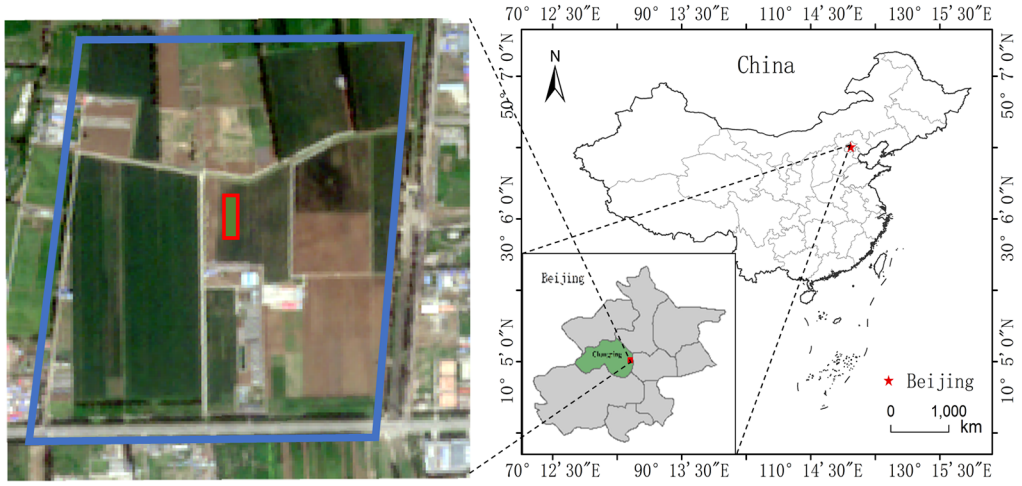

Fig. 1 Geographical location of the study area.

Table 1 Summary of cultivar, treatments, and samples for the experiment.

Data	Growth period	Number of samples	Cultivar, treatments, and unfolded blades of each plant			
			J-N0	J-N2	Z-N0	Z-N2
August 6, 2017	V12	37	9	11	8	9
August 17, 2017	VT	47	12	13	10	12
August 31, 2017	R3	39	9	10	8	12

Note: J-N0 indicates that the cultivar was Jingke968 and treatment was 0 kg/hm^2; Z-N2 indicates that the cultivar was Zhengdan958 and treatment was 420 kg/hm^2; J-N2 and Z-N0 indicate the same as above.

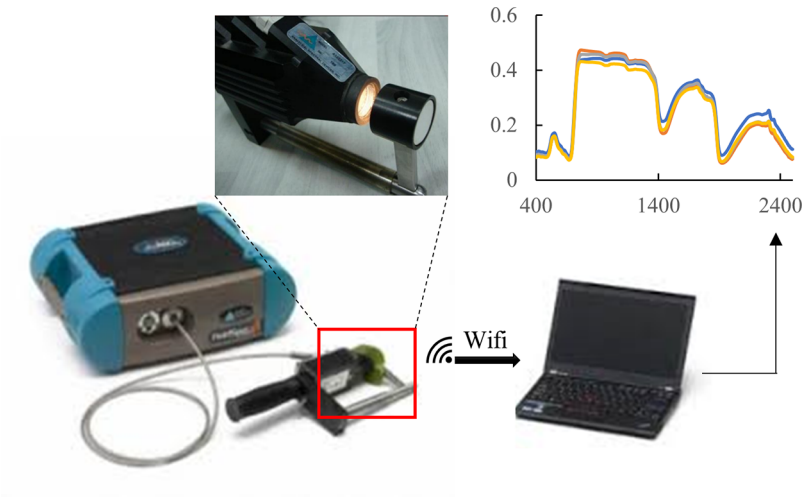

Fig. 2 Spectrum collection of maize leaves.

available potassium content is 86.83 to 120.62 mg/kg, and organic matter content is 15.8 to 20.0 g/kg.

The experiment is a complete randomized design with two maize cultivars (Jingke968 and Zhengdan958) and two urea fertilizer applications rates (0 and 420 kg/hm^2) (Table 1). Four plots were set up, and one maize plant was collected in each plot. Maize plants were brought back to the laboratory, and leaves were collected from different layers from the top to bottom. Urea fertilizer was applied at the growth stages of V6 and V12. Other management procedures, such as pest management, weed control, and phosphate and potassium fertilizers, followed the local standard practices for maize production.

2.1.1 *Determination of leaf spectrum*

At the growth stages of V12, VT, and R3 of summer maize, a completely representative plant was selected from each plot and brought back to the laboratory. The stems and leaves were separated and each piece of unfolded leaf was tested and marked. Leaf spectral measurements were taken using a FieldSpec FR2500 spectroradiometer (Analytical Spectral Devices Inc., Boulder, Colorado) coupled with an ASD Leaf Clip, an accessory of the ASD spectroradiometer (Fig. 2). The spectral range was 350 to 2500 nm, the resolution was 1.4 nm in the range of 350 to 1000 nm and 2 nm in the range of 1000 to 2500 nm, and the spectral resampling interval was 1 nm. The ASD Leaf Clip was clamped on the central position of the vein during measurement. The mean of the four reflectance curves was taken as the leaf reflectance spectral curve, and the mean of the other four transmittance curves was obtained as the leaf transmittance spectral curve. The model used in this study was PROSPECT, which can simulate at the spectral range of 400 to 2500 nm. Therefore, the SR in the range of 400 to 2500 nm was obtained as the actual measurement value for the leaf spectrum.

2.1.2 *Acquisition of agronomic parameters*

We selected the position of the sample spectrum to measure the LCC value by using a Dualex 4 nitrogen balance index meter (Force-A, Orsay, France). The maize LCC measurements are in one-to-one correspondence with the spectral curves of the leaves. The paper bag containing the sample was placed in the oven. The temperature was set to 105°C for 30 min and then adjusted to 80°C, and the leaves were finally dried to a constant weight (about 24 to 48 h). The following are the calculation methods for equivalent water thickness (Ewt) and dry matter content (D_m)

$$\mathrm{Ewt(cm)} = \frac{\mathrm{FWL(g)} - \mathrm{DWL(g)}}{\mathrm{LA(cm^2)} * \mathrm{D(g/cm^3)}} \times 100\%, \tag{1}$$

$$D_m(\mathrm{g/cm^2}) = \frac{\mathrm{DWL(g)}}{\mathrm{LA(cm^2)}}, \tag{2}$$

where FWL is the fresh weight of the leaves, D is the water density, which is usually 1 $\mathrm{g/cm^3}$, DWL is the dry weight of the leaves, and LA is the leaf area of collected samples.

2.2 *PROSPECT-D Model*

The PROSPECT model is a radiation transfer model used to calculate the hemispherical reflectivity and transmittance of one blade and can simulate the optical properties of plant leaves from 400 to 2500 nm. The original PROSPECT-1 model was proposed by Jacquemoud and Baret in 1990.[10] In this model, the spectral absorption coefficient can be expressed as

$$K(\lambda) = \sum K_i(\lambda), \tag{3}$$

where λ is the wavelength (400 to 2500 nm, step size is 1 nm), $K(\lambda)$ is the spectral absorption coefficient of the blade, $K_i(\lambda)$ is the spectral absorption coefficient of the relative leaf component i, and C_i is the content of the leaf component i per unit leaf area.

This study was based on the PROSPECT-D model. The input parameters and abbreviations of the model are shown in Table 2. The range of each input parameter of the PROSPECT model was set according to the physical and chemical properties of the maize, and those based on previous research experience to optimize the ill-conditioned inversion of the model.[30,31] The PROSPECT-D model used the following equations to calculate the effect of each blade component on the SR:

$$\begin{aligned} K(\lambda) = \frac{1}{N}[&K_{\mathrm{LCC}}(\lambda) * \mathrm{LCC} + K_{\mathrm{Lcar}}(\lambda) * \mathrm{Lcar} + K_{\mathrm{Lcant}}(\lambda) * \mathrm{Lcant} + K_{\mathrm{Lbrown}}(\lambda) * \mathrm{Lbrown} \\ &+ K_{Dm}(\lambda) * Dm + K_{\mathrm{Ewt}}(\lambda) * \mathrm{Ewt}], \end{aligned} \tag{4}$$

where $K_{\mathrm{LCC}}(\lambda)$ is the absorption coefficient of LCC, $K_{\mathrm{Lcar}}(\lambda)$ is the absorption coefficient of Lcar, $K_{\mathrm{Lcant}}(\lambda)$ is the absorption coefficient of Lcant, $K_{\mathrm{Lbrown}}(\lambda)$ is the absorption coefficient of Lbrown, $K_{Dm}(\lambda)$ is the absorption coefficient of Dm, and $K_{\mathrm{Ewt}}(\lambda)$ is the absorption coefficient of Ewt.

2.3 *Vegetative Index*

Thirteen vegetation indices related to leaf chlorophyll were selected according to the spectral characteristics of summer maize and previous research results (Table 3). Sensitivity analysis was performed on these VI and LCC, and the vegetation indices sensitive to LCC and insensitive to other parameters were selected for the comparison characteristics of cost function.

Table 2 Input variables and their range in the PROSPECT-D model.

Model	Variable	Abbreviation	Bounds
PROSPECT-D	Leaf structure parameter	*N*	1 to 5
	Leaf chlorophyll content (μg/cm^2)	LCC	10 to 70
	Leaf carotenoid content (μg/cm^2)	Lcar	0 to 10
	Lear anthocyanin content (μg/cm^2)	Lcant	0 to 1
	Leaf brown pigment content (μg/cm^2)	Lbrown	0 to 1
	Equivalent water thickness (cm)	Ewt	0 to 0.06
	Dry matter content (g/cm^2)	Dm	0.0028 to 0.0054

Table 3 Summary of VI.

VI	Name	Formula	References
DCNI	Double-peak canopy nitrogen index	$(R_{720}-R_{700})/\frac{R_{700}-R_{670}}{(R_{720}-R_{670}+0.03)}$	32
EVI	Enhanced VI	$\frac{2.5(R_{800}-R_{670})}{(1+R_{800}+6R_{670}-7R_{479})}$	33
EVI2	Two-band EVI	$\frac{2.5(R_{800}-R_{660})}{(1+R_{800}+2.4R_{660})}$	34
GNDVI	Green normalized difference VI	$(R_{750}-R_{550})/(R_{750}+R_{550})$	35
MCARI	Modified chlorophyll absorption ratio index	$[R_{700}-R_{670}-0.2*(R_{700}-R_{550})]*(R_{700}/R_{670})$	36
MSAVI	Modified soil-adjusted VI	$0.5\left[2R_{800}+1-\sqrt{(2R_{800}+1)^2-8(R_{800}-R_{670})}\right]$	37
MTVI2	Modification of the triangle VI2	$\frac{1.5[1.2(R_{800}-R_{500}-2.5(R_{670}-R_{550}))]}{\sqrt{2(R_{800}+1)^2-\left[6R_{800}-5\sqrt{R_{670}}\right]-0.5}}$	38
NDVI	Normalized difference VI	$(R_{890}-R_{670})/(R_{890}+R_{670})$	39
NDVI g-b	Normalized difference VI green-blue	$(R_{573}-R_{440})/(R_{573}+R_{440})$	40
$NDVI_{canste}$	NDVI Canste	$(R_{760}-R_{708})/(R_{760}+R_{708})$	41
NPCI	Normalized pigment chlorophyll VI	$(R_{430}-R_{680})/(R_{430}+R_{680})$	42
PPR	Plant pigment ratio	$(R_{550}-R_{450})/(R_{550}+R_{450})$	43
TCARI	Transformed chlorophyll absorption in reflectance index	$3*(R_{710}-R_{680})-0.2*(R_{700}+R_{560})*(R_{710}/R_{680})$	44

Notes: VI represents the vegetation index.

2.4 *Methods*

2.4.1 *EFAST*

The EFAST method is a quantitative global sensitivity analysis method based on variance and combines the advantages of the Sobol method and Fourier amplitude method by Saltelli et al.[45] The basic idea of the algorithm comes from the Bayesian theorem,[46,47] that is, the sensitivity of the model output can be reflected by the variance of the model results. The parameter sensitivity is divided into the following two types by decomposing the variance of the parameters on the model results: the influence of a single parameter on the results and that of the coupling between the parameters on the model results. The single parameter independent action is measured by the main effect index, whereas the parameter interaction is measured by the difference between the total effect and the main effect.[48] Assuming that the model was $y = f(x_1, x_2, \ldots x_k)$, the search curve function Gi could be converted to $y = f$ (s),[49] and $f(s)$ was Fourier transformed as

$$\begin{aligned} y = f(s) &= \sum_{i=-\infty}^{\infty} \{A_j \cos(is) + B_j \sin(is)\}, \\ A_i &= \frac{1}{N_s} \sum_{k=1}^{N_s} f(s_k) \cos(\omega_i s_k), \\ B_i &= \frac{1}{N_s} \sum_{k=1}^{N_s} f(s_k) \sin(\omega_i s_k), \end{aligned} \tag{5}$$

where N_s is the number of samples, $i \in \overline{Z} = \{-\frac{N_s-1}{2}, \ldots, -1, 0, 1, \ldots + \frac{N_s-1}{2}\}$.

The spectral curve of the Fourier series is defined as $\Lambda = A_i^2 + B_i^2$, and the variance of the model results caused by the change of the parameter x_i is

$$V_i = 2 \sum_{i=1}^{+\infty} \Lambda_i \omega_i. \tag{6}$$

According to the decomposition model of the Sobol method, the total variance of the model output could be decomposed into a function of a single parameter and combined parameters

$$V = \sum_{i=1}^{k} V_i + \sum_{i \neq j}^{k} V_{ij} + \sum_{i \neq j \neq m}^{k} V_{ijm} + \ldots + V_{1,2,\ldots,k}, \tag{7}$$

where V_i is the model variance caused by the individual change of input parameter x_i, $V_{ij}, V_{ijm}, \ldots, V_{1,2,\ldots,k}$ are the variances of the interactions of the various parameters, and k is the number of parameters. Afterward, the direct contribution of the parameter x_i to the total variance of the model output can be reflected by the main effect index S_i (first-order sensitivity index). The first-order sensitivity index Si of the parameter x_i is normalized by processing

$$S_i = \frac{V_i}{V}. \tag{8}$$

The total effect of the parameter x_i is

$$S_{Ti} = \frac{V - V_{-i}}{V}, \tag{9}$$

where V_i is the sum of the variances of all parameters, excluding the parameter x_i.

According to previous research and experience,[13] the bounds for each input variable of the PROSPECT-D model were set (Table 2). A total of 8000 sets of variables were randomly simulated using the Monte Carlo method, and 8000 spectral curves were simulated using the PROSPECT-D model. Sensitivity analysis was performed using these simulated data and their

transformed forms. Only 400 to 1000 nm analysis was selected to facilitate the selection of sensitive features.

2.4.2 *Continuous wavelet transform*

The CWT is a linear transformation method that decomposes hyperspectral data into a series of WC at different scales by using the wavelet basis functions. The transformation equation[24] is as follows:

$$W_f(a,b) = \langle f, \Psi_{a,b} \rangle = \int_{-\infty}^{+\infty} f(\lambda)\Psi_{a,b}(\lambda)\mathrm{d}\lambda, \tag{10}$$

$$\Psi_{a,b}(\lambda) = \frac{1}{\sqrt{a}}\Psi\left(\frac{\lambda - b}{a}\right), \tag{11}$$

where $f(\lambda)$ is the hyperspectral reflectance data, λ is the spectral band (400 to 2500 nm), $\Psi_{a,b}$ is the wavelet basis function, a is the scale factor, and b is the translation factor. WC contains two dimensions, namely, i and j, which are $m \times n$ matrices composed of decomposition scales ($i = 1,2,\ldots,m$) and bands ($j = 1,2,\ldots,n$). Thus, CWT converts one-dimensional hyperspectral reflectance data into two-dimensional WC.[50]

In this paper, the Meyer function[51] with fast convergence rate was selected as the wavelet base, and 8000 simulated reflectivity curves were transformed by CWT using MATLAB. The decomposition scale of CWT was set to $2^1, 2^2, 2^3, \ldots, 2^{10}$ (corresponding to scales 1, 2, 3, ..., 10) to reduce data redundancy.

2.4.3 *Gradient descent inversion algorithm*

The gradient descent algorithm is an iterative method commonly used for efficient problem optimization. In this method, the extremum of the function is searched by the direction along the gradient. A cost function must be introduced to determine the quality of the calculation results.[52] The model variable (Va) is predicted by constructing the cost function. The difference between the model-simulated spectral characteristics and the measured spectral characteristics was calculated. The cost function is as follows:

$$f(Va) = \sqrt{\frac{1}{n}\sum (CT_{\text{prospect}} - CT_{\text{leaf}})^2}, \tag{12}$$

where n is the number of selected VI, CT_{prospect} is the set of spectral characteristics calculated from the SR of the blades simulated by the PROSPECT-D model, and CT_{leaf} is the set of spectral characteristics calculated from the actual measured leaf reflectance.

The gradient descent algorithm is used to reverse the PROSPECT-D model. The original parameters of the model (e.g., LCC) can be calculated by taking the spectral characteristics of the leave positions at different plant heights as the input parameter. In addition, the parameters of model inversion can be restricted by setting the interval of each parameter (Table 2) and combining it with the above cost function, and the extreme value of the model inversion can be ignored. In this manner, the model inversion can obtain high precision.

2.5 *Statistical Analysis*

Coefficient of determination (R^2), mean absolute deviation (MAD), mean difference (MD), and normalized root mean squared error (nRMSE) are used to evaluate the pros and cons of the model. MAD is the average of the absolute values of the deviations of all individual observations from the arithmetic mean. The errors cancelling one another can be avoided, thus implying that the actual prediction error can be accurately reflected.[53] MD is the difference between the average measured and predicted data. MD > 0 indicates "underestimation," and MD < 0 indicates "overestimation."[54] nRMSE generally gives a substantial difference limit when describing

the accuracy of the model. For example, nRMSE <10% means no difference, 10% ≤ nRMSE < 20% means small difference, 20% ≤ nRMSE < 30% means medium difference, and nRMSE ≥ 30% means large difference.[55] The formulas for MAD, MD, and nRMSE are as follows:

$$\mathrm{MD} = \overline{y_i} - \overline{y_j}, \tag{13}$$

$$\mathrm{MAD} = \frac{1}{n}\sum_{i=1}^{n} |y_i - y_j|, \tag{14}$$

$$\mathrm{nRMSE} = \frac{\sqrt{\frac{\sum_{i=1}^{n}(y_i - y_j)^2}{n}}}{\overline{y_i}}, \tag{15}$$

where y_i is the measured value, y_j is the predicted value, $\overline{y_i}$ is the average of the measured values, $\overline{y_j}$ is the average of the predicted values, and n is the number of samples.

3 Results

3.1 *Selection of Cost Function Features*

EFAST sensitivity analysis of LCC was performed to determine the reflectivity of simulated data at 400 to 1000 nm. The sensitive range of LCC is shown in Fig. 3. The total effect index of each parameter varies greatly in different bands. The band with a relatively high total effect index of LCC mainly appears at 400 to 500 and 570 to 710 nm. The top 10% of the total effect index was used to construct the cost function of the model inversion, in which the total effect index was higher than 0.955 and the corresponding sensitive band was 637 to 698 nm.

The EFAST sensitivity analysis of 13 VI indicates that $\mathrm{NDVI}_{\mathrm{canste}}$ (0.997) obtained the best sensitivity, whereas EVI (0.006) obtained the worst sensitivity (Fig. 4). Based on the $\mathrm{NDVI}_{\mathrm{canste}}$ inversion, we found that the total effect index of LCC was the highest, whereas the total effect index of the other parameters was negligible. For other vegetation indices, except for LCC, the other parameters yielded different effects on the model results. In addition, EVI, EVI2, MSAVI, and MTVI2 were extremely sensitive to Lbrown. In our future work, we will extract the content of Lbrown or eliminate its influence by using the above indices. In this study, the $\mathrm{NDVI}_{\mathrm{canste}}$ with the highest effect index was used to construct the cost function of the model inversion.

CWT was used to decompose the simulated hyperspectrum (Fig. 5). The band with the relatively high total effect index mainly appeared at 600 to 850 nm, and the corresponding decomposition scale was 1 to 8. The WC of the top 1% effect index was used to construct

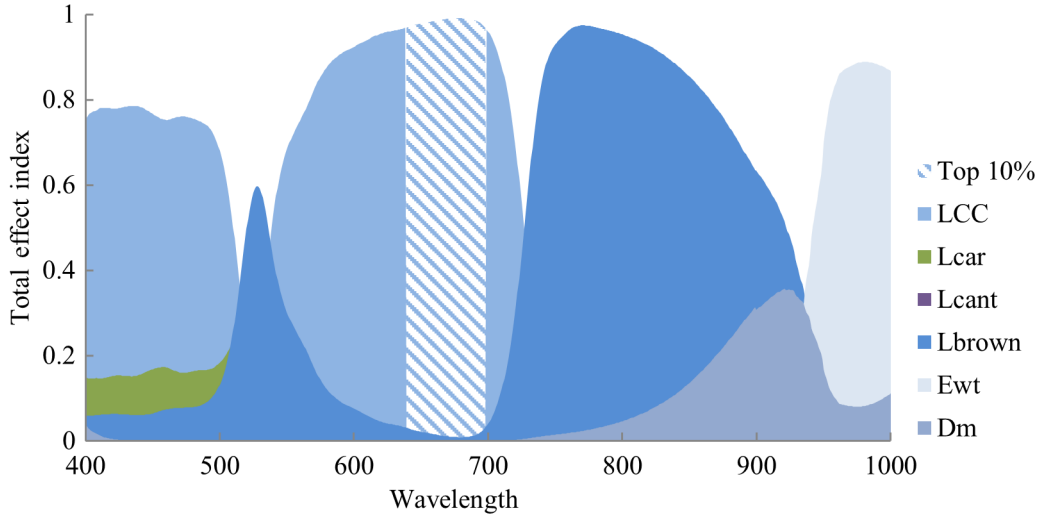

Fig. 3 Sensitivity analysis of SR and input variables of PROSPECT-D.

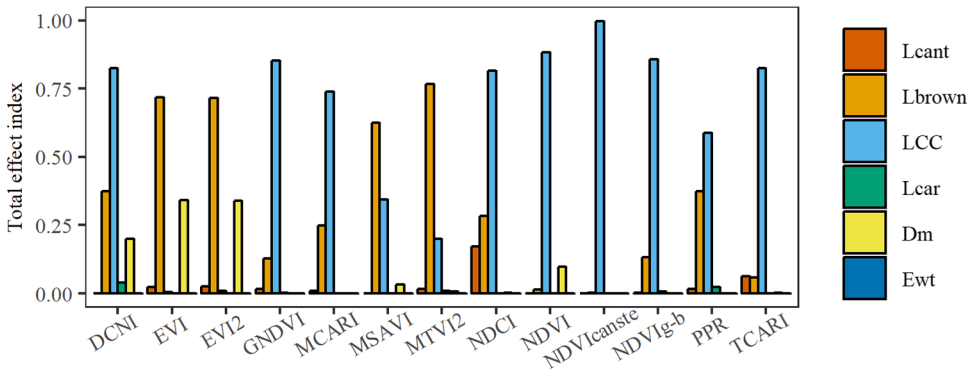

Fig. 4 Sensitivity analysis of VI and input variables of PROSPECT-D.

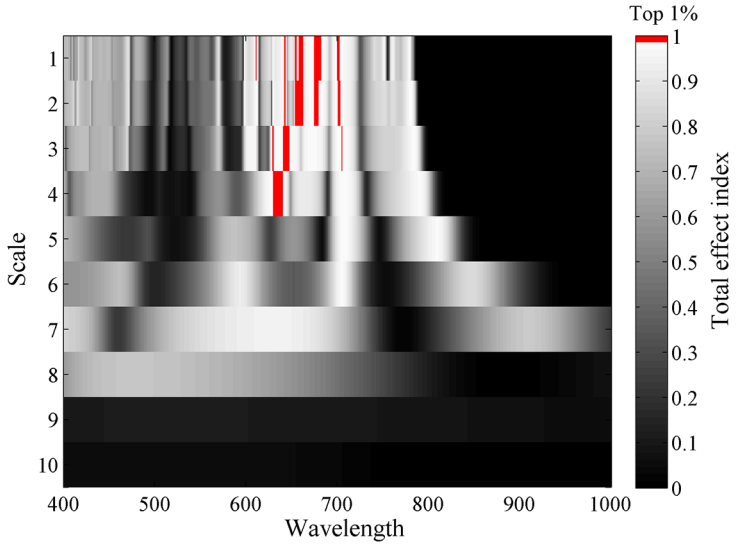

Fig. 5 Sensitivity analysis of WC and LCC.

the cost function of the model inversion. The selected WC values were mainly concentrated in the ranges of 607 to 612, 625 to 650, 654 to 662, 668 to 686, 697 to 713, 778 to 793, and 806 to 812 nm, and the corresponding decomposition scale was 1 to 4. The selected WC corresponded to the sensitive band in Fig. 3, but the corresponding bands were few. The selected band contained more information than the original band.

3.2 *PROSPECT-D Model for LCC Estimation*

The inversion results of LCC are shown in Fig. 6. The accuracy of SR as the cost-function inversion of LCC was poor, with R^2 and nRMSE of 0.348 and 59.3%, respectively. The MD predicted by SR was 22.48 $\mu g/cm^2$, indicating severe "underestimation." The margin line in Fig. 6 intuitively explains the disadvantage of SR prediction. The prediction results differed from the measured results. The R^2 values of the accuracies of $NDVI_{canste}$ and WC as the cost-function inversions of LCC were 0.826 and 0.782, respectively, and both reached the significant level ($p < 0.01$). Although the accuracy of using $NDVI_{canste}$ as the cost function was higher than that using WC, the prediction results moderately differed from the measured results with nRMSE of 27.07% and MD of -8.89 $\mu g/cm^2$, indicating "overestimation." The prediction results of using WC as the cost function slightly differed from the measured results, with nRMSE and MD of 16.47% and 4.3 $\mu g/cm^2$, respectively. The MADs predicted by VI and WC were 9.19 and 5.47 $\mu g/cm^2$, respectively. The bias measure of WC prediction was less than that of VI prediction. As discussed above, $NDVI_{canste}$ can weaken and simultaneously reflect the influence of other biochemical parameters on SR change; this relation can serve as basis for

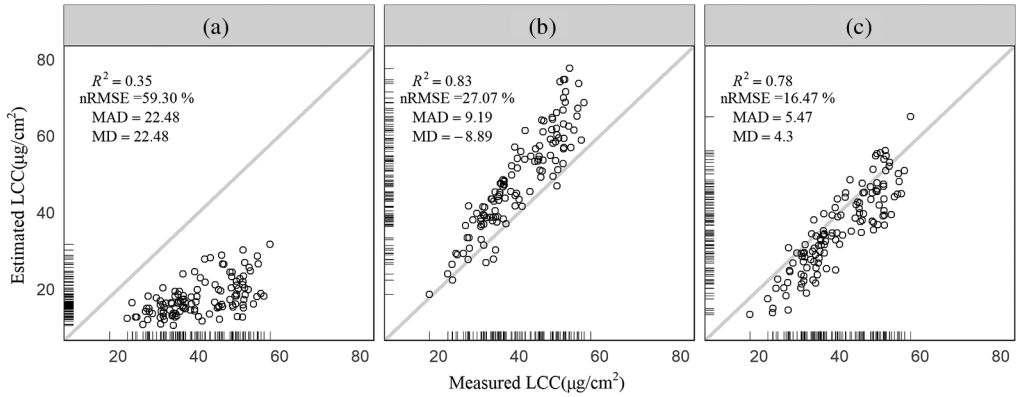

Fig. 6 Relationship between measured and estimated LCC by PROSPECT-D model: (a) SR-based results, (b) VI-based results, and (c) WC-based results.

improving the inversion precision of the physical model. The CWT method can eliminate the interference information between the bands, improve the accuracy of the inversion, and extract the weak information among the spectra. The performance of this method, combined with the physical model in PROSPECT, is better than that by using sensitive band and VI.

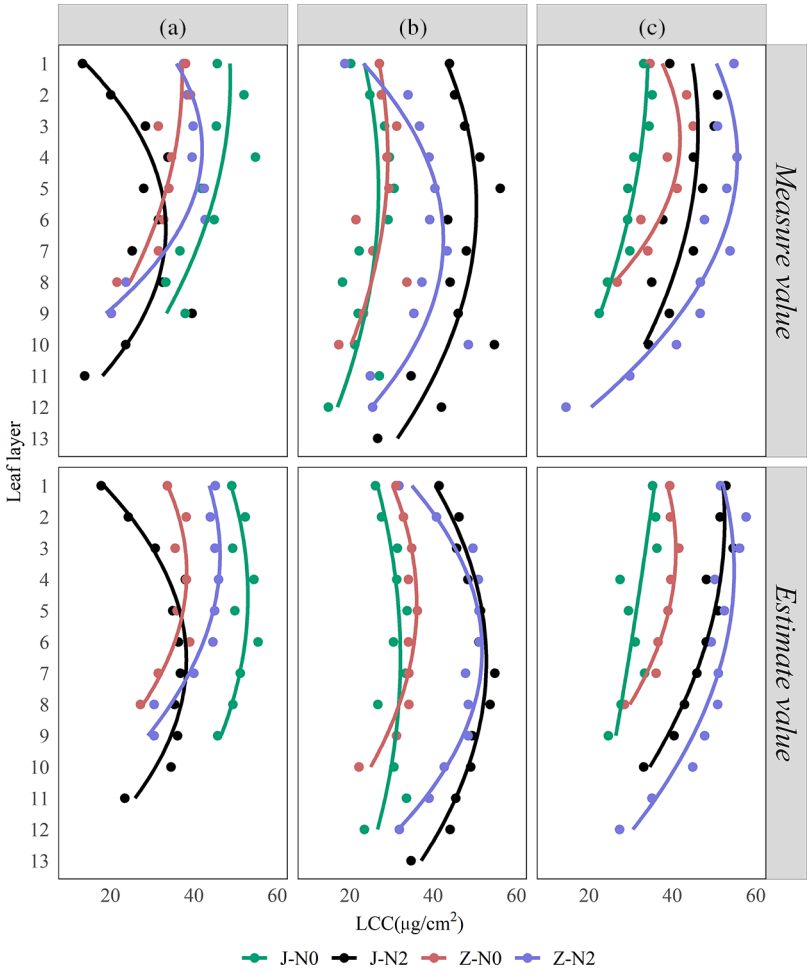

Fig. 7 Layered point diagram of LCC measured and LCC estimated by CWT algorithm: (a) V12, (b) VT, and (c) R3. Note: The vertical coordinates represent the leaf layer of maize leaves from top to bottom. J and Z represent the two varieties of Jingke968 and Zhengdan958, and N0 and N2 represent two nitrogen fertilizer applications, respectively.

3.3 *Nonuniform Vertical LCC Distribution in Maize*

Note: The vertical coordinates represent the leaf layer of maize leaves from top to bottom. J and Z represent the two varieties of Jingke968 and Zhengdan958, and N0 and N2 represent two nitrogen fertilizer applications, respectively.

The measured LCC and estimated LCC vertical distributions of maize from top to bottom at the growth stages of V12, VT, and R3 are shown in Fig. 7. LCC was estimated by using the inversion algorithm of WCs. During the three growth stages, LCC showed a nonuniform vertical distribution and changed across different growth stages. The trend is parabolic for the initial increase and decrease from top to bottom, and R^2 showed a significant difference, which proves the existence of vertical distribution differences among different leaf positions of maize due to chlorophyll translocation. In addition, the LCC at the bottom of the plant is lower than that LCC at the top, indicating that chlorophyll loss originated from the bottom layer. Remote sensing monitoring was incomplete because only upper spectral information was obtained to monitor the entire canopy. At the growth stages of VT and R3, the LCC of each leaf position of the two maize plants with normal fertilization was significantly higher than that without fertilization. However, at the growth stages of V12, no significant difference exists between fertilization and nonfertilization. A possible reason is that urea has just been applied and is not working yet.

4 Discussion

The PROSPECT-D model was used to estimate the LCC of maize. The results reveal that SR transformations differ in terms of LCC inversion performance, indicating that hyperspectral remote sensing monitoring can have great potential for mining. Compared with the traditional empirical and semiempirical methods,[56,57] the proposed method exhibits a strong mechanism while maintaining the best possible accuracy. Mao et al.[58] and Li et al.[59] successfully estimated the chlorophyll content of plants and achieved excellent results. However, their methods only established a single relationship between spectrum and chlorophyll and did not consider the combined effects of spectrum and various factors. The theoretical strength of this study is attributed to the physicochemical relationships and interactions among multiple factors (i.e., carotenoids, anthocyanins, and water) when extracting chlorophyll information.

Analyzing the sensitivity of physical modeling parameters is a prerequisite of model inversion. The physical model is mainly high-dimensional and nonlinear, and its parameters may be dependent; thus, the sensitivity analyses of the parameters tend to be complex.[60] EFAST is a typical quantitative global sensitivity analysis method. The overall influence of LCC, Lcar, and other parameters on the results of PROSPECT-D model for *SR*, VI, and WC was investigated, and the influence of the interaction on the parameters and that of the parameters on the modeling results were analyzed. The proposed method screened a range of selected bands, including the results of the chlorophyll inversion models of Song et al.[61] and Yang et al.,[62] which were sensitive to LCC but insensitive to other parameters. Moreover, the screening of band reflectance, VI and WCs helped refine the analytic process and reflect the sensitivity changes with different characteristics.

The LCC inversion of maize leaves was conducted by using the sensitive band as the cost function of inversion algorithm. The accuracy of the results was poor, the deviation was large, and severe underestimation was perceived. These findings may be attributed to the large amount of unknown interference information between adjacent bands that cannot be removed.[63] Another possibility is that the band reflectance has not been subdivided, thus neglecting some useful information. The inversion algorithm that used VI as an input feature of cost function effectively improved the inversion accuracy of LCC. $NDVI_{canste}$ with the greatest contribution of LCC and the least contribution from the other parameters were screened out by using EFAST global sensitivity analysis. This method embodied the advantages of VI in LCC inversion,[36,64] and effectively reduced the interference of other parameters on the results. The inversion algorithm based on the CWT effectively improved the inversion accuracy of LCC and greatly reduced the deviation. The complex composition of leaves resulted in a large number of weak information in the SR of chlorophyll. WCs filtered by EFAST can effectively eliminate the interference

information between bands. On this basis, CWT can effectively separate useful information from weak information, thus leading to efficient utilization of available information.

The vertical heterogeneity of LCC in different growth stages of summer maize was observed, and LCC showed a parabolic trend that first increased and then decreased from the top layer; this trend is in accordance to the general law of vertical distribution of LCC in crop canopy.[5] The vertical heterogeneity was due to the different light environments, functional leaf positions of plants, and nitrogen uptake. At the growth stages of VT and R3, the LCC of fertilized maize was significantly higher than that of nonfertilized maize, indicating that LCC is directly related to fertilization. However, the difference was not evident at the growth stage of V12, because fertilization treatment was performed at the growth stages of V6 and V12, and urea may not have played a role in the samples collected at the growth stage of V12. After VT, the maize leaves began to enter a growth transition period, and the old leaves at the bottom level turned yellow and withered. This phenomenon resulted in the general absence of bottom leaves during the R3 growth period. The LCC was extremely low even for the Z-N2 plants that were not initially considered. The phenomenon of the bottom layer having fewer leaves than the top layer is difficult to monitor by remote sensing. Traditional remote sensing monitoring uses chlorophyll and its uniform distribution in the canopy, but this scheme cannot meet the accuracy requirements. In future research, the vertical heterogeneity of chlorophyll may be used to modify the traditional remote sensing quantitative monitoring model. In addition, the vertical heterogeneity of LCC became inverted relative to the ROSPECT-D model based on CWT, and the measured LCC was consistent with the distribution law. These findings suggest that the model can successfully estimate the LCC of maize and sufficiently reveal the vertical distribution of LCC. Vertical distribution data can be used to monitor microchange information at the bottom level of the maize field and subsequently regulate the crop nutrient information over time. In the future, we will comprehensively analyze the relationship between radiation transfer and vertical distribution and explore the subtle changes of nutrients in the field by using physical models.

5 Conclusion

A cost function was constructed in this study by using the SR, VI, and WC of sensitive bands, and LCC was inverted by the PROSPECT-D model. The major conclusions are as follows.

1. Sensitive LCC wavebands were mainly concentrated at 637 to 698 nm. $NDVI_{canste}$ was more sensitive than other VIs. The sensitive bands with continuous wavelet decomposition were mainly concentrated at 607 to 612, 625 to 650, 654 to 662, 668 to 686, 697 to 713, 778 to 793, and 806 to 812 nm, and the corresponding decomposition scale was 1 to 4.
2. VI and CWT calculations can effectively separate useful information from weak information and improve their utilization, implying the improved inversion accuracy of LCC ($R^2 = 0.826$ and 0.782). CWT (nRMSE = 16.47%, MAD = 5.47, MD = 4.3) can also help extract weak information among spectra and is a better approach than VI (nRMSE = 27.07%, MAD = 9.19, MD = −8.89). Priority is given to the combination of PROSPECT-D model and CWT to obtain crop nutrient information at the field level.
3. The LCC distributions of different maize varieties and treatments have a parabolic trend from top to bottom, and R^2 is significant. The CWT-based PROSPECT-D model can satisfactorily the law. For maize with different treatments, LCC with normal fertilization is significantly higher than LCC without fertilization. This finding has great theoretical importance in the study of vertical heterogeneity, which is typically observed with the response of different leaf position spectra to LCC. In actual field management, this rule can be used to examine subtle changes in the different positions of a vertical profile rather than just focusing on poststress management.

Acknowledgments

This work was supported by the National Key Technologies of Research and Development Program (Grant Nos. 2016YFD0300602 and 2017YFD0201501); SDUST Research Fund

(Grant No. 2019TDJH103); the Beijing Natural Science Foundation (Grant No. 6182011); Programme for Beijing Excellent Talents in Organization Department of Beijing Municipal Party Committee (Grant No. 2017000020060G128); Natural Science Foundation of Beijing Academy of Agriculture and Forestry Sciences (Grant No. QNJJ201834). We also would like to thank the anonymous reviewers for providing constructive suggestions to improve the manuscript.

References

1. Y. Li et al., "The robustness of linear regression model in rice leaf chlorophyll concentration prediction," *J. Remote Sens.* **7**(5), 364–371 (2003).
2. G. Vane and A. F. H. Goetz, "Terrestrial imaging spectrometry: current status, future trends," *Remote Sens. Environ.* **44**(2–3), 117–126 (1993).
3. K. S. Fassnacht et al., "Estimating the leaf area index of north central Wisconsin forests using the Landsat thematic mapper," *Remote Sens. Environ.* **61**(2), 229–245 (1997).
4. V. Ciganda, A. Gitelson, and J. Schepers, "Non-destructive determination of maize leaf and canopy chlorophyll content," *J. Plant Physiol.* **166**(2), 157–167 (2009).
5. L. Winterhalter, B. Mistele, and U. Schmidhalter, "Assessing the vertical footprint of reflectance measurements to characterize nitrogen uptake and biomass distribution in maize canopies," *Field Crops Res.* **129**(1), 14–20 (2012).
6. J. Hailing et al., "Research on spectral scale effect in the estimation of vegetation leaf chlorophyll content," *Spectrosc. Spectral Anal.* **36**(1), 169–176 (2016).
7. D. A. Sims and J. A. Gamon, "Relationships between leaf pigment content and spectral reflectance across a wide range of species, leaf structures and developmental stages," *Remote Sens. Environ.* **81**(2), 337–354 (2002).
8. J. Pisek and J. M. Chen, "Comparison and validation of MODIS and VEGETATION global LAI products over four BigFoot sites in North America," *Remote Sens. Environ.* **109**(1), 81–94 (2007).
9. C. Y. Wu et al., "An evaluation of EO-1 hyperspectral Hyperion data for chlorophyll content and leaf area index estimation," *Int. J. Remote Sens.* **31**(4), 1079–1086 (2010).
10. S. Jacquemoud and F. Baret, "PROSPECT: a model of leaf optical properties spectra," *Remote Sens. Environ.* **34**(2), 75–91 (1990).
11. J. B. Féret et al., "PROSPECT-D: towards modeling leaf optical properties through a complete lifecycle," *Remote Sens. Environ.* **193**, 204–215 (2017).
12. C. Wei et al., "Estimation and mapping of winter oilseed rape LAI from high spatial resolution satellite data based on a hybrid method," *Remote Sens.* **9**(5), 488 (2017).
13. C. Camino et al., "Improved nitrogen retrievals with airborne-derived fluorescence and plant traits quantified from VNIR-SWIR hyperspectral imagery in the context of precision agriculture," *Int. J. Appl. Earth Obs. Geoinf.* **70**, 105–117 (2018).
14. L. Wu et al., "Simulation of vegetation indices optimizing under retrieval of vegetation biochemical parameters based on PROSPECT+SAIL model," *Chin. J. Appl. Ecol.* **23**(12), 3250–3256 (2012).
15. S. Zhaoming and Y. Cungui, "Global sensitivity analysis for affecting factors of firing dispersion of multiple launch rockets system based on EFAST method," *Ordnance Ind. Autom.* **37**(10), 95–99 (2018).
16. C. Xu et al., "Sensitivity analysis in ecological modeling," *Chin. J. Appl. Ecol.* **15**(6), 1056 (2004).
17. A. Saltelli, S. Tarantola, and P. S. Chan, "A quantitative model-independent method for global sensitivity analysis of model output," *Technometrics* **41**(1), 39–56 (1999).
18. J. Wu et al., "Global sensitivity analysis of growth simulation parameters of winter wheat based on EPIC model," *Trans. Chin. Soci. Agric. Eng.* **25**(7), 136–142 (2009).
19. Q. Ren, Y. Chen, and X. Shu, "Global sensitivity analysis of Xinanjiang model parameters based on extend FAST method," *Acta Sci. Nat. Univ. Sunyatseni* **49**(3), 127–134 (2010).
20. J. Zhiwei, C. Zhongxin, and R. Jianqiang, "The inversion of vegetation leaf area index based on the canopy radiative transfer model ACRM," *Chin. J. Agric. Resour. Reg. Plann.* **32**(01), 57–63 (2011).

21. P. Bowyer and F. M. Danson, "Sensitivity of spectral reflectance to variation in live fuel moisture content at leaf and canopy level," *Remote Sens. Environ.* **92**(3), 297–308 (2004).
22. G. L. Maire et al., "Leaf area index estimation with MODIS reflectance time series and model inversion during full rotations of Eucalyptus plantations," *Remote Sens. Environ.* **115**(2), 586–599 (2011).
23. Y. Lei et al., "Inversion of soil organic matter content using hyperspectral data based on continuous wavelet transformation," *Spectrosc. Spectral Anal.* **36**(5), 1428–1433 (2016).
24. T. Cheng, B. Rivard, and G. A. Sánchez-Azofeifa, "Spectroscopic determination of leaf water content using continuous wavelet analysis," *Remote Sens. Environ.* **115**(2), 659–670 (2011).
25. Q. Liao et al., "Comparison of spectral indices and wavelet transform for estimating chlorophyll content of maize from hyperspectral reflectance," *J. Appl. Remote Sens.* **7**(1), 073575 (2013).
26. P. J. Curran et al., "Reflectance spectroscopy of fresh whole leaves for the estimation of chemical concentration," *Remote Sens. Environ.* **39**(2), 153–166 (1992).
27. Z. Wang et al., "Vertical distribution of nitrogen in different layers of leaf and stem and their relationship with grain quality of winter wheat," *J. Plant Nutr.* **28**(1), 73–91 (2005).
28. Y. Guo et al., "Exploring the vertical distribution of structural parameters and light radiation in rice canopies by the coupling model and remote sensing," *Remote Sens.* **7**(5), 5203–5221 (2015).
29. J. Luo et al., "Estimating the total nitrogen concentration of reed canopy with hyperspectral measurements considering a non-uniform vertical nitrogen distribution," *Remote Sens.* **8**(10), 789 (2016).
30. R. H. Byrd, J. C. Gilbert, and J. Nocedal, "A trust region method based on interior point techniques for nonlinear programming," *Math. Program.* **89**(1), 149–185 (2000).
31. J. Jiang et al., "Estimation of leaf traits from reflectance measurements: comparison between methods based on vegetation indices and several versions of the PROSPECT model," *Plant Methods* **14**(1), 23 (2018).
32. P. F. Chen et al., "New spectral indicator assessing the efficiency of crop nitrogen treatment in corn and wheat," *Remote Sens. Environ.* **114**(9), 1987–1997 (2010).
33. E. Boegh et al., "Airborne multispectral data for quantifying leaf area index, nitrogen concentration, and photosynthetic efficiency in agriculture," *Remote Sens. Environ.* **81**(2–3), 179–193 (2002).
34. Z. Jiang et al., "Development of a two-band enhanced vegetation index without a blue band," *Remote Sens. Environ.* **112**(10), 3833–3845 (2008).
35. F. Baret and G. Guyot, "Potentials and limits of vegetation indices for LAI and APAR assessment," *Remote Sens. Environ.* **35**(2–3), 161–173 (1991).
36. C. S. T. Daughtry et al., "Estimating corn leaf chlorophyll concentration from leaf and canopy reflectance," *Remote Sens. Environ.* **74**(2), 229–239 (2000).
37. J. Qi et al., "A modified soil adjusted vegetation index," *Remote Sens. Environ.* **48**(2), 119–126 (1994).
38. D. Haboudane et al., "Hyperspectral vegetation indices and novel algorithms for predicting green LAI of crop canopies: modeling and validation in the context of precision agriculture," *Remote Sens. Environ.* **90**(3), 337–352 (2004).
39. R. L. Pearson and L. D. Miller, "Remote mapping of standing crop biomass for estimation of the productivity of the shortgrass prairie," in *Proc. Eighth Int. Symp. Remote Sens. Environ.*, Vol. VIII, p. 1355 (1972).
40. P. M. Hansen and J. K. Schjoerring, "Reflectance measurement of canopy biomass and nitrogen status in wheat crops using normalized difference vegetation indices and partial least squares regression," *Remote Sens. Environ.* **86**(4), 542–553 (2003).
41. K. Steddom et al., "Remote detection of rhizomania in sugar beets," *Phytopathology* **93**(6), 720–726 (2003).
42. A. A. Gitelson and M. N. Merzlyak, "Signature analysis of leaf reflectance spectra: algorithm development for remote sensing of chlorophyll," *J. Plant Physiol.* **148**(3–4), 494–500 (1996).

43. G. Metternicht, "Vegetation indices derived from high-resolution airborne videography for precision crop management," *Int. J. Remote Sens.* **24**(14), 2855–2877 (2003).
44. C. G. Pettersson and H. Eckersten, "Prediction of grain protein in spring malting barley grown in northern Europe," *Eur. J. Agron.* **27**(2–4), 205–214 (2007).
45. A. Saltelli et al., *Sensitivity Analysis in Practice: A Guide to Assessing Scientific Models*, pp. 20–78, John Wiley and Sons, New York (2004).
46. P. C. Yan et al., "The analysis of the influence of globe SST anomalies on 500 hPa temperature field based on Bayesian," *Acta Phys. Sin.* **61**(13), 139202 (2012).
47. C. Q. Hao, "Estimating topology of complex networks based on sparse Bayesian learning," *Acta Phys. Sin.* **61**(14), 148901 (2012).
48. L. He et al., "Global sensitivity analysis of APSIM-wheat parameters in different climate zones and yield levels," *Trans. Chin. Soc. Agric. Eng.* **31**(14), 148–157 (2015).
49. Y. Li, C. Huang, and L. Lu, "Global sensitivity analysis of SEBS model parameters based on EFAST method," *Remote Sens. Technol. Appl.* **29**(5), 719–726 (2014).
50. Q. Liao et al., "Estimation of fluvo-aquic soil organic matter content from hyperspectral reflectance based on continuous wavelet transformation," *Trans. Chin. Soc. Agric. Eng.* **28**(23), 132–139 (2012).
51. I. Daubechies and C. Heil, *Ten Lectures on Wavelets* National Defense Industry Press, Beijing (1992).
52. G. Yuedong and S. Xudong, "Analysis and improvement of gradient descent method," *Technol. Outlook* **26**(15), 115–117 (2016).
53. J. Junping et al., *Statistics*, 4th ed., p. 374, China Renmin University Press (CRUP), Beijing (2009).
54. J. Przyborowski and H. Wileński, "The ratio of the mean deviation to the standard deviation as a test of normality," *Biometrika* **27**(3/4), 310–332 (1935).
55. J. Timsina and E. Humphreys, "Performance of CERES-rice and CERES-wheat models in rice-wheat systems: a review," *Agric. Syst.* **90**, 5–31 (2006).
56. X. Yao et al., "Exploring hyperspectral bands and estimation indices for leaf nitrogen accumulation in wheat," *Int. J. Appl. Earth Obs. Geoinf.* **12**(2), 89–100 (2010).
57. L. Wang and Y. Wei, "Revised normalized difference nitrogen index (NDNI) for estimating canopy nitrogen concentration in wetlands," *Optik* **127**(19), 7676–7688 (2016).
58. Z. H. Mao et al., "Research on the application of UAV multispectral remote sensing in the maize chlorophyll prediction," *Spectrosc. Spectral Anal.* **38**(09), 2923–2931 (2018).
59. L. Yongliang, "GA-BP neural network estimation models of chlorophyll content based on red edge parameters and PCA," *Sci. Silvae Sin.* **48**(09), 22–29 (2012).
60. W. He and H. Yang, "EFAST method for global sensitivity analysis of remote sensing model's parameters," *Remote Sens. Technol. Appl.* **28**(5), 836–843 (2013).
61. K. Song et al., "A hyperspectral model for estimating chlorophyll content in maize leaves," *Acta Agron. Sin.* **31**(8), 1095–1097 (2005).
62. J. Yang et al., "Hyperspectral estimation model for chlorophyll concentrations in top leaves of rice," *Acta Ecol. Sin.* **29**(12), 6561–6571 (2009).
63. R. He et al., "Retrieving canopy leaf total nitrogen content of winter wheat by continuous wavelet transform," *Trans. Chin. Soc. Agric. Eng.* **31**(2), 141–146 (2015).
64. C. Wu et al., "Estimating chlorophyll content from hyperspectral vegetation indices: modeling and validation," *Agric. For. Meteorol.* **148**(8–9), 1230–1241 (2008).

Xiaobin Xu received his MS degree in surveying and mapping engineering from Shandong University of Science and Technology in 2019. His research interests include radiation transmission models, agricultural quantitative remote sensing analysis, and quality prediction.

Zhenhai Li received his PhD in agricultural remote sensing and information technology from Zhejiang University, Hangzhou, China, in 2016. He is currently an assistant professor with Beijing Research Center for Information Technology in Agriculture, Beijing Academy of Agriculture and Forestry Sciences, Beijing, China. His current research interests include remote sensing analysis and diagnosis of crop growth and nitrogen, crop yield and quality forecasting by assimilating crop growth model, and remote sensing.

Xiaodong Yang received his PhD in cartography and geographic information systems from the State Key Laboratory of Remote Sensing Science, Institute of Remote Sensing Applications, Chinese Academy of Sciences. His research interests are in agricultural remote sensing and geographic information systems.

Guijun Yang received his PhD in cartography and geographic information systems from the State Key Laboratory of Remote Sensing Science, Institute of Remote Sensing Applications, Chinese Academy of Sciences, in 2008. He is currently a research associate with the National Engineering Research Center for Information Technology in Agriculture, Beijing, China. His research interests cover radiative transfer modeling, imagery simulation, atmospheric correction, quantitative inversion, and land cover change monitoring.

Cong Teng is a graduate student in the School of Surveying and Mapping of Shandong University of Science and Technology. His research interests are agricultural remote sensing and feature classification.

Hongchun Zhu received his PhD in photogrammetry and remote sensing from Northwestern University in 2008. He is currently an associate professor at the School of Surveying and Mapping of Shandong University of Science and Technology. He is mainly engaged in GIS applications, remote sensing image processing and analysis, digital elevation models and digital terrain analysis, and other aspects of teaching and research work.

Shuaibing Liu received his MS degree in surveying and mapping engineering from Henan Polytechnic University in 2019. His research interests include quantitative remote sensing of agriculture and monitoring of plant growth.